ACS APPLIED MATERIALS & INTERFACES

Research Article

Cite This: ACS Appl. Mater. Interfaces 2019, 11, 31508−31519

www.acsami.org

Hierarchical Morphology of Poly(ether ether ketone) Aerogels

Samantha J. Talley,[†,⊥] Stephanie L. Vivod,[‡] Baochau A. Nguyen,[§] Mary Ann B. Meador,[‡] Aurel Radulescu,[∥] and Robert B. Moore*[,†]

[†]Department of Chemistry, Macromolecules Innovation Institute (MII), Virginia Tech, Blacksburg, Virginia 24061, United States

[‡]NASA Glenn Research Center, 21000 Brookpark Road, Cleveland, Ohio 44135, United States

[§]Ohio Aerospace Institute, 22800 Cedar Point Road, Cleveland, Ohio 44142, United States

[∥]Jülich Center for Neutron Science, JCNS Outstation at MLZ, Forschungszentrum Jülich GmbH, Lichtenbergstrasse 1, Garching 85747, Germany

Supporting Information

ABSTRACT: The phase diagram for the thermoreversible gelation of poly(ether ether ketone) (PEEK) in 4-chlorophenol (4CP) was constructed over broad temperature and concentration ranges, revealing that PEEK is capable of dissolving and forming gels in both 4CP and dichloroacetic acid (DCA) up to a concentration of 25 wt %. Highly porous aerogels of PEEK were prepared through simple solvent exchange followed by one of two drying methods of solvent removal from the wet gel: freeze-drying or supercritical CO_2 fluid extraction (SC-drying). The field-emission scanning electron microscopy analysis showed that gelation of PEEK in 4CP, followed by SC-drying, produced aerogels with well-defined lamellar aggregates as compared to less ordered aggregates formed from DCA. Mechanical properties (in compression) were shown to improve with increasing density, resulting in equivalent compressive moduli at comparable density, regardless of the preparation method (gelation solvent selection, concentration variation, or drying method). Nitrogen adsorption−desorption isotherms indicate that PEEK aerogels are comprised of mesopores (2−50 nm diameter pores) formed from stacked crystalline lamella. PEEK aerogels prepared using SC-drying exhibit higher Brunauer−Emmett−Teller surface areas than freeze-dried aerogels of comparable density. The ultra-small-angle X-ray scattering/small-angle X-ray scattering (SAXS)/wide-angle X-ray scattering analysis revealed a hierarchical morphology of the PEEK aerogels with structural features from PEEK crystallites to agglomerates of stacked lamella that spanned a wide range of length scales. SANS contrast-matching confirmed that the morphological origin of the principle scattering feature in PEEK aerogels is stacked crystalline lamella. Nitrogen sorption measurements of porosity and the specific surface area of the PEEK aerogels were correlated with the SAXS analysis to reveal a remarkably high surface area attributed to the platelet-like, lamellar morphology. Contact angle and contact angle hysteresis (CAH) revealed that low-density PEEK aerogels (ρ < 0.15 g/cm^3) have water contact angles above the superhydrophobicity cutoff angle (>150°) and a very low CAH near 1°.

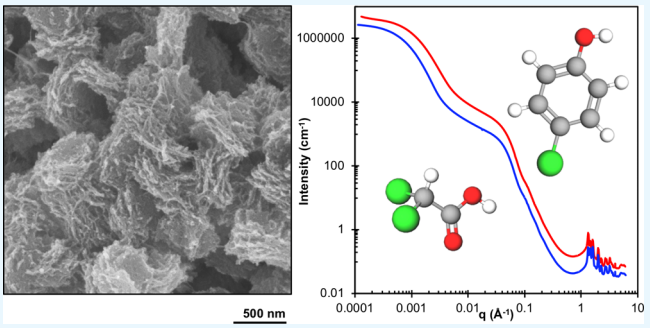

KEYWORDS: *aerogel, physical gelation, PEEK, semicrystalline, small-angle scattering*

INTRODUCTION

Thermoreversible gels are a class of solid-like materials, often referred to as physical gels, consisting of a three-dimensional network comprised of thermally labile cross-links that are capable of confining large volume fractions of solvent. In the case of thermoreversible polymer gels, the physical network can be formed through reversible aggregation phenomena such as crystallization, ionic aggregation, phase separation, hydrogen bonding, complex formation, or helix formation.[1,2] The liquid or gaseous solvent is retained within the macromolecular framework, and the gel possesses solid-like, elastic material properties.[3] Although many semicrystalline polymers exist, relatively few have been shown to form thermoreversible gels. Recently, we have reported the gelation of poly(ether ether ketone) (PEEK) in dichloroacetic acid (DCA)[4,5] and herein present the discovery of a new solvent, 4-chlorophenol (4CP), that is also capable of forming monolithic, thermoreversible gels of PEEK.

Thermoreversible gelation of semicrystalline polymers is often not limited to a single gelation solvent. Semicrystalline polymers such as poly(vinyl chloride),[6] poly(methyl methacrylate),[7−9] polyethylene,[10,11] isotactic polypropylene,[12] poly(vinylidene fluoride) (PVDF),[13,14] and poly(4-meythylpentene-1),[15−18] and stereoregular polystyrene[19] gel thermorever-

Received: June 3, 2019
Accepted: August 5, 2019
Published: August 5, 2019

DOI: 10.1021/acsami.9b09699
ACS Appl. Mater. Interfaces 2019, 11, 31508−31519

sibly in more than one solvent. In the case of syndiotactic polystyrene (sPS), thermoreversible gelation proceeds in many solvents including chloroform,[20,21] toluene,[20−22] benzene,[21,23] bromoform,[24] octadecyl benzoate,[25] chlorotetradecane,[26] *o*-dichlorobenzene,[21,22] 1,2,4-trichlorobenzene,[27] tetrahydrofuran,[22] trichloroethylene,[21] 1,2-dichloroethane,[21,26] and others. In the case of these physical, semicrystalline gels, the gelation solvent often influences the resulting gel morphology[6,28] and crystal structure of polymorphic polymers, particularly sPS.[29]

When the solvent is removed from a wet gel by means of simple evaporation, the resulting dry material, called a xerogel, does not retain the porosity and specific morphology of the wet gel.[30] However, when the solvent removal from the wet gel is carefully controlled without perturbing the wet gel morphology, a highly porous aerogel is produced.[31] Aerogels are typically utilized in applications that require materials with a high surface area, low density, and high porosity such as thermal insulation,[32,33] battery electrodes,[34,35] catalyst supports,[36,37] oil−water emulsion separation,[38] and filtration processes.[39] These applications take advantage of the low density and high surface area of aerogels, and thus, it is crucial to understand the relationship between the porous aerogel morphology and aerogel fabrication processes.

The techniques commonly utilized for aerogel drying are freeze-drying and supercritical fluid extraction.[30] In the freeze-drying method, the solvent within the liquid gel is frozen and removed via sublimation. Freeze-drying is a facile, inexpensive technique, but the formation of solvent crystals during the freezing process can significantly impact the resulting morphology of the aerogel.[40] Poorly controlled freeze-drying, resulting in evaporation in addition to sublimation, often leads to pore collapse and material densification, similar to that of a xerogel. Unlike freeze-drying, supercritical fluid extraction does not rely on solvent freezing and sublimation processes. When an aerogel is prepared by supercritical fluid extraction, the solvent in the wet gel is exchanged for a supercritical fluid, most commonly supercritical CO_2. Following solvent exchange, temperature and pressure are returned to atmospheric conditions and the supercritical fluid imbibed in the gel network transitions to a gaseous state, resulting in an aerogel comprised of the dry, but otherwise unaltered, gel morphology. Although supercritical drying is regarded as the most reliable drying method to prepare aerogels, the facile freeze-drying process is commonly used because supercritical fluid extraction is often costly, time-consuming, and hazardous, requiring specialized high-pressure instrumentation.[40,41]

In this work, a new solvent capable of forming monolithic, thermoreversible gels of PEEK is introduced. Extending upon our previous work on thermoreversible gels of PEEK from DCA, the impact of the gelation solvent (4CP vs DCA) and drying technique (freeze-drying vs supercritical fluid extraction) on the resulting gel morphology and physical properties of semicrystalline PEEK gels is compared. Morphological features of the resulting gels are compared using scanning electron microscopy (SEM) and various scattering methods. To elucidate the morphological origins of scattering features of PEEK gels and aerogels, the powerful SANS contrast-matching method is employed. Following scattering feature identification, detailed information extracted from the small-angle X-ray scattering (SAXS) analysis regarding the interfacial surface morphology may be correlated with direct measurements using nitrogen adsorption techniques.

EXPERIMENTAL SECTION

Materials. PEEK (Victrex V150P) was provided by Solvay Specialty Polymers (Alpharetta, GA). DCA (>99.0%) and 4CP (>99%) were purchased from Sigma-Aldrich (Saint Louis, MO). Ethanol (200 proof, 100% USP, Decon Labs), magnesium sulfate (anhydrous), deuterium oxide (D_2O, 99.8%), and syringes (3 mL, plastic, luer lock, nonsterile) were purchased from Fisher Scientific Company LLC (Suwanee, GA). Syringe filters (GE Healthcare, 30 mm, PTFE, 5.0 μm) were purchased from VWR International LLC (Radnor, PA).

Preparation of PEEK Gels. DCA was dried over magnesium sulfate and filtered using PTFE syringe filters, and 4CP was used as received. PEEK (V150P unless otherwise specified) was dissolved in dry DCA at 185 °C or 4CP at 205 °C. Complete dissolution took place between 1 and 2 h for concentrations significantly lower than 15 wt % and up to 24 h for concentrations over 15 wt %. The solutions were removed from the 185 or 205 °C oil bath, drawn into syringes and immediately transferred to controlled-temperature water or sand baths for isothermal gelation. The gelation temperatures ranged from 10 to 140 °C (DCA) or 50 to 140 °C (4CP). The lower temperature limit was defined to avoid the solvent freezing point. Solutions that gelled formed a firm, light brown, opaque gel that did not flow when the syringe was inverted, passing the tip test. Gelation was monitored frequently, and gelation times were recorded at the first instance of passing the tip test.[4]

For SANS experiments, DCA-type gels were solvent-exchanged with H_2O, D_2O, or a mixture of H_2O/D_2O using a soxhlet extractor set to 100 °C and cycled for 3 days to completely replace DCA with H_2O, D_2O, or a mixture of H_2O/D_2O. The 4CP-type gels were solvent-exchanged with ethanol using a soxhlet extractor set to 100 °C and cycled for 3 days to completely replace 4CP with ethanol. The gels were then solvent-exchanged with H_2O, D_2O, or a mixture of H_2O/D_2O using a soxhlet extractor set to 100 °C and cycled for 3 days to completely replace ethanol with an aqueous solvent.

Aerogel Preparation. Syringes containing gelled PEEK in DCA or 4CP were cut near the luer lock. The gels were then gently removed from the syringes through the cut opening without disrupting the cylindrical gel geometry. The DCA-type gels were immediately placed in water for a period of 24 h, then solvent-exchanged with water using a soxhlet extractor set to 100 °C, and cycled for 3 days to completely replace DCA with water. The 4CP-type gels were immediately placed in ethanol for a period of 24 h, then solvent-exchanged with ethanol using a soxhlet extractor set to 100 °C, and cycled for 3 days to completely replace 4CP with ethanol. The gels were then solvent-exchanged with water using a soxhlet extractor set to 100 °C and cycled for 3 days to completely replace ethanol with water. Once the gels contained only PEEK and water, they were frozen overnight at −18 °C and subsequently lyophilized (LabConco) to produce freeze-dried PEEK aerogels. DCA and 4CP-type gels were also solvent-exchanged to ethanol using soxhlet extraction (at 100 °C) for a period of 3 days to completely convert to ethanol-only gels and then dried using supercritical fluid extraction, followed by drying under vacuum at 80 °C overnight to ensure complete solvent removal.

Morphological Analysis. The aerogel morphology was analyzed using field-emission SEM (FE-SEM) using a LEO (Zeiss) 1550 FE-SEM with in-lens detection. All specimens were sputter-coated with iridium (5 nm thickness) in a Leica EM ACE600 sputter coater. Ultra-small-angle X-ray scattering (USAXS)/SAXS/wide-angle X-ray scattering (WAXS) measurements were collected at beam line 9-ID-C at the Advanced Photon Source (APS) at Argonne National Laboratory (Lemont, Illinois).[42,43] SAXS and WAXS profiles were reduced using the Nika program for Igor Pro.[44] The Irena program for Igor Pro was used to reduce USAXS profiles and merge same-specimen USAXS SAXS and WAXS profiles.[45] Scattering data were normalized in terms of absolute intensity using glassy carbon.[46] USANS and SANS measurements were collected at beam line KWS-2 operated by the Julich Centre of Neutron Science (JCNS) at the Heinz Maier-Leibnitz Center (MLZ) (Garching, Germany).[47] Data

DOI: 10.1021/acsami.9b09699
ACS Appl. Mater. Interfaces 2019, 11, 31508−31519

were collected at multiple sample-to-detector distances and neutron wavelengths (λ = 5, 10 Å in pinhole; λ = 7 Å in focusing geometries) in order to cover a wide wave vector transfer range, 0.0001 < q < 0.5 Å^{-1}.[48] Wet gel samples were loaded in 300 μL quartz cells and held at a temperature of 293 K. After the standard correction and calibration procedure was applied using the QtiKWS data reduction software,[48] the 2-D data were azimuthally integrated leading to the 1-D scattered intensity (in absolute units of cm^{-1}).

Characterization of Physical Properties. Mechanical properties of cylindrical aerogel specimens were tested in accordance with ASTM D695-10 using a model 5867 Instron equipped with a 30 kN load cell. Samples were nominally 16 mm in height and 8 mm in diameter, complying with the 2:1 ratio of height to diameter prescribed for compression testing of polymer foams. The nitrogen adsorption porosimetry analysis was conducted at NASA Glenn Research Center (Cleveland, OH) using an ASAP 2000 Surface Area/Pore Distribution analyzer (Micromeritics Instrument Corp). All samples were outgassed at 80 °C for 24 h prior to the nitrogen adsorption analysis. Contact angle measurements were performed using the sessile drop method on a contact angle goniometer (ramé-hart model 590) and its software package (DROPimage Advanced).

RESULTS AND DISCUSSION

Gelation of PEEK in 4CP. In our previous reports, we demonstrated that PEEK is capable of forming monolithic thermoreversible gels from 8−25 wt % DCA solutions.[4,5] We have recently found that PEEK is also capable of forming monolithic, thermoreversible gels from 4CP solutions. Similar to the gelation behavior of PEEK/DCA, the PEEK/4CP gelation phenomena is best presented using a three-dimensional phase diagram (Figure 1) configured to display

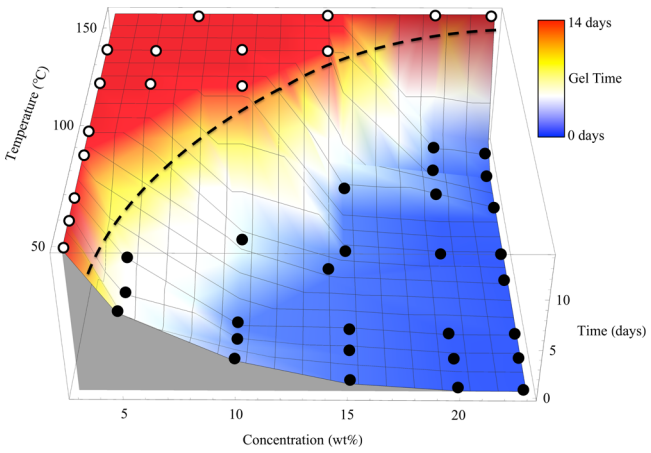

Figure 1. Time-dependent sol−gel phase diagram of PEEK in 4CP, where the gel time is displayed along the z-axis ranging from less than 1 day (blue) to no gel after 14 days (red). Solutions that did not gel within 14 days are designated as open circles (◯); solutions that gelled within 14 days are shown as filled circles (●).

concentration, temperature, and time with respect to gelation. The phase diagram experimentally determined for PEEK/4CP gelation is notably similar to that of PEEK/DCA in that the upper boundary of gelation (at high temperatures and high polymer concentration) is consistent with an upper critical solution temperature (UCST) behavior and the lower boundary (at low temperature and low polymer concentration) is restricted by the solvent freezing point. At high concentrations, gelation proceeds rapidly, within a matter of minutes, whereas at low concentrations and temperatures, gelation proceeds much more slowly. The similar gelation behavior of PEEK/DCA and PEEK/4CP (and similar morphological features of the gels, see below) suggests a common mechanism of gelation for both solvents. Generally, semicrystalline polymers that are capable of forming gels from solution undergo the sol−gel transformation following a temperature jump (in this case to a temperature below the UCST) by a mechanism involving a liquid−liquid phase separation by spinodal decomposition followed by crystallization of chain segments in the polymer-rich phase,[19] ultimately developing a percolated,[49] solvent-swollen network structure. Future in-situ scattering experiments defining the structural development during gelation will be required to confirm this general mechanism and fully understand the similarities in gel morphology between these two solvent−polymer systems.

SEM of PEEK Aerogels. The morphology of freeze-dried PEEK/DCA gels was recently shown by SEM to be comprised of fractal-like uniform globular features decorated with smaller nodules.[4,5] Because gel morphology can be significantly affected by the choice of the gelling solvent, it is of interest here to characterize and compare the morphology of the new PEEK/4CP gels to PEEK/DCA gels that were prepared in a similar fashion. Figure 2 shows the FE-SEM micrographs of

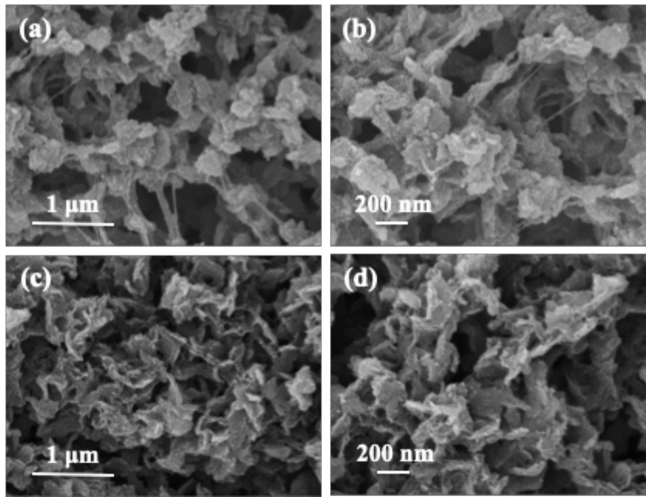

Figure 2. FE-SEM micrographs of the freeze-dried PEEK aerogels prepared from 15 wt % PEEK in DCA (a,b) or 4CP (c,d).

freeze-dried PEEK/DCA and PEEK/4CP aerogels. It is clear from these data that the new PEEK/4CP aerogels are also comprised of agglomerates of a fairly uniform dimension and size comparable to that observed in the PEEK/DCA gels. In contrast, however, the agglomerates in the freeze-dried PEEK/4CP aerogels are clearly more platelet-like as opposed to the globular forms observed in the PEEK/DCA gels. While freeze-drying is known to cause pore collapse and densification in aerogels, it is important to note that both the PEEK/DCA and PEEK/4CP gels were freeze-dried under identical conditions (i.e., both were converted to hydrogels prior to freeze-drying). Thus, it is unlikely that the platelet morphology of the PEEK/4CP gels is solely attributed to structural disruption arising from the freeze-drying process.

As a common alternative to freeze-drying, supercritical fluid extraction (SC) using supercritical CO_2 was also utilized to prepare PEEK aerogels from PEEK/DCA and PEEK/4CP gels to determine the influence of the drying technique on the

DOI: 10.1021/acsami.9b09699
ACS Appl. Mater. Interfaces 2019, 11, 31508−31519

aerogel morphology. The morphologies of the SC-dried PEEK/DCA and PEEK/4CP aerogels, shown in Figure 3,

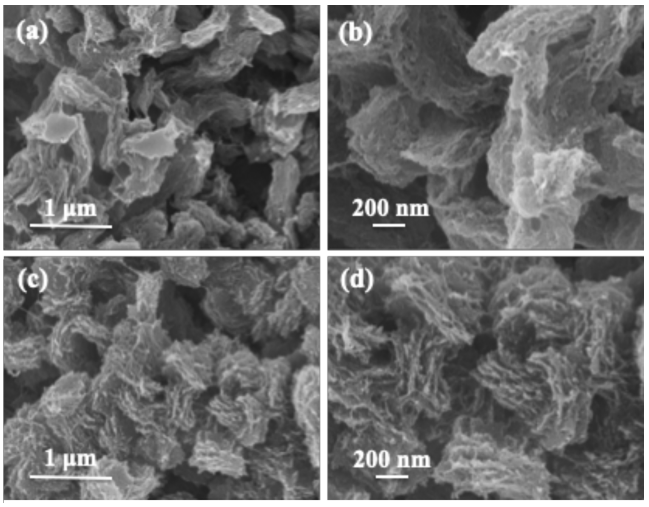

Figure 3. SEM micrographs of PEEK aerogels dried using supercritical fluid extraction. Aerogels were prepared from 15 wt % PEEK in DCA (a,b) or 4CP (c,d).

are comprised of significantly larger morphological features than the freeze-dried analogues in Figure 2. The difference in size of the morphological features can be attributed to the challenges inherent to the freeze-drying technique, resulting in pore collapse and densification of features. It is reasonable then to conclude that SC-drying minimally perturbs the gel network as compared to freeze-drying, such that the morphology observed in SC-dried aerogels is a more accurate representation of the wet gel morphology.

With less disruptive solvent extraction afforded by SC-drying, it is apparent that the finer details of the semicrystalline morphology of the gels are preserved. The morphologies of SC-dried PEEK aerogels from both gelation solvents (Figure 3) appear to consist of large aggregates of stacked crystalline lamellae of limited lateral dimensions. In comparison of the two gelling solvents, it is clear that lamellae are much more defined in the micrographs of SC-dried PEEK/4CP aerogels, but lamellar features are still present in the SC-dried PEEK/DCA aerogels. Overall, the morphological features present in SC-dried PEEK/DCA aerogels appear to be comprised of more densely packed lamellar aggregates than the expanded stacks present in SC-dried PEEK/4CP. With the more refined lamellar structure created in the PEEK/4CP gels, it is now apparent that the compact platelet structures observed in the freeze-dried PEEK/4CP gels (Figure 2c,d) originate from a compaction of the lamellar stacks during solvent freezing and/or extraction. Nevertheless, this profound compaction is only possible given the well-ordered lamellar structure formed by gelation in 4CP.

Based on previous studies of thermoreversible gelation of semicrystalline PVDF, the enhanced order of the PEEK lamella formed from 4CP, relative to those from DCA, may be attributed to differences in polymer−solvent interactions during gelation. Okabe and co-workers investigated the gelation phenomenon of PVDF with respect to the magnitude of the Flory−Huggins interaction parameters of various PVDF/solvent pairs.[50] For solvents with interaction parameters in the vicinity of $\chi_{sp} \approx 0.5$, thermoreversible gelation was prevalent. Moreover, conformational ordering and subsequent crystallization during the sol−gel transition in these solvents was found to be particularly sensitive to the magnitude of χ_{sp}. The polymer chains in solvents with larger interaction parameters (i.e., relatively poorer solvents) were found to crystallize rapidly during gelation. In contrast, for solvents with smaller interaction parameters, where polymer−solvent interactions are more favorable, gelation by crystallization was found to occur more slowly. Thus, assuming that the general gelation mechanism of PEEK is similar between DCA and 4CP, and typical of other semicrystalline polymers (i.e., liquid−liquid phase separation, followed by crystallization), it is reasonable to consider the contribution of the Flory−Huggins interaction parameters in the phase separation and crystallization processes with these two solvents.

With the knowledge of the Hansen solubility parameters of the solvents and polymer, δ_s and δ_p, the Flory−Huggins solvent/polymer interaction parameter, χ_{sp}, may be estimated using the following empirical relationship

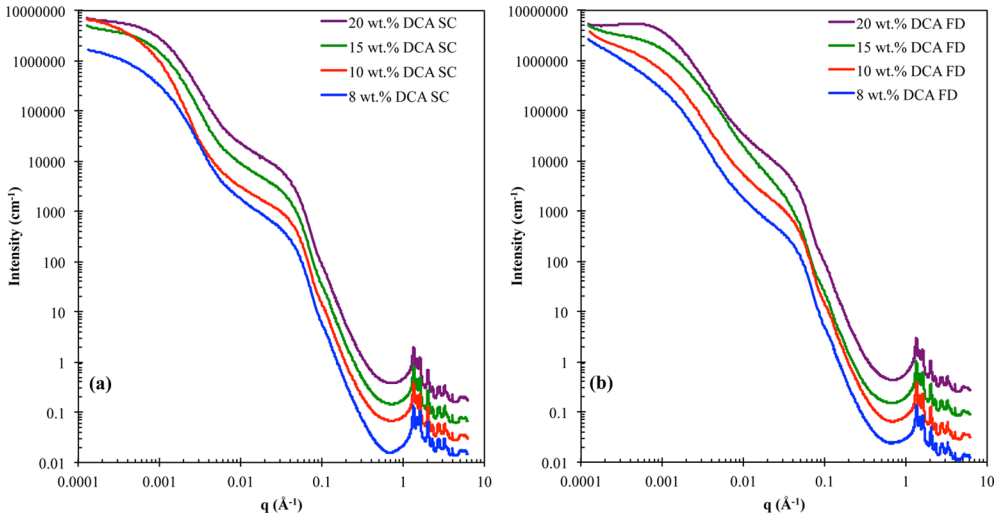

Figure 4. USAXS/SAXS/WAXS profiles of PEEK aerogels prepared by SC-drying (a) or freeze-drying (b) gels of various concentrations (wt %) of PEEK in DCA. Profiles offset vertically for comparison.

DOI: 10.1021/acsami.9b09699
ACS Appl. Mater. Interfaces 2019, 11, 31508−31519

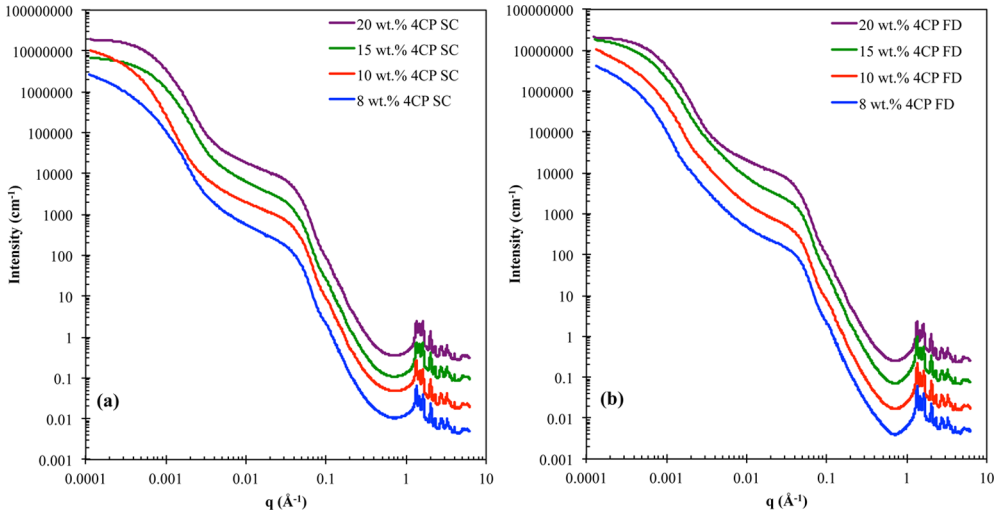

Figure 5. USAXS/SAXS/WAXS profiles of PEEK aerogels prepared by SC-drying (a) or freeze-drying (b) gels of various concentrations (wt %) of PEEK in 4CP. Profiles offset vertically for comparison.

$$\chi_{sp} = 0.34 + \frac{V_s(\delta_p - \delta_s)^2}{RT} \quad (1)$$

where V_s is the molar volume of the solvent, R is the gas constant, T is the absolute temperature, and the correction factor of 0.34 accounts for entropic contributions stemming from a mismatch in free volumes of the low molecular weight liquid and the inherently connected polymer units.[51] The solubility parameters of DCA,[52] 4CP,[53] and PEEK[54] are reported to be 22.5, 25.2, and 26.4 $MPa^{1/2}$, respectively. Using the molar volumes of 8.3×10^{-5} and 9.85×10^{-5} m^3/mol for DCA and 4CP, respectively, the interaction parameter at 50 °C for the DCA/PEEK solution is estimated to be $\chi_{DCA/PEEK}$ = 0.461, and for the 4CP/PEEK solution, $\chi_{4CP/PEEK}$ = 0.384. Comparison of these values suggests that 4CP is a somewhat better solvent for PEEK than DCA. Therefore, following the findings of Okabe,[50] it is reasonable to suspect that more favorable polymer−solvent interactions would facilitate slower growth in the development of more ordered crystalline lamella in 4CP, as observed in Figure 3.

SAXS and SANS Analysis of the Hierarchical Morphology in PEEK Aerogels. Hierarchical solids, such as aerogels, contain structural elements which are comprised of a subsequent structure on a smaller scale.[55] Scattering techniques have long been used to characterize the microstructure of porous, hierarchically ordered aerogel materials.[56,57] Often, complex scattering profiles of aerogels originate from a highly porous, mass fractal network of solid agglomerates of structural features. As anticipated from the SEM analysis above, the scattering behavior of PEEK aerogels also yields significant scattering complexity over a wide range of length scales attributed to the apparent hierarchical morphology.

USAXS/SAXS/WAXS experiments were performed on PEEK aerogels prepared by SC-drying or freeze-drying PEEK/DCA and PEEK/4CP gels. The scattering profiles of aerogels prepared from four concentrations of PEEK/DCA gels and PEEK/4CP gels are shown in Figures 4 and 5. Regardless of the solvent, gel concentration, or solvent extraction method, the scattering profiles of all of the aerogels generally show the same principle features: (1) a USAXS Guinier knee centered near q = 0.001 $Å^{-1}$, (2) a second SAXS knee centered near q = 0.035 $Å^{-1}$, and (3) WAXD Bragg reflections, q > 1 $Å^{-1}$, characteristic of the semicrystalline nature of PEEK. Using the WAXD data, the degree of crystallinity of the gels was determined by standard deconvolution methods (Figure S1). For the DCA gels, the degree of crystallinity, % X_c, was found to range from ca. 35 to 37%, and for the 4CP gels, % X_c, was found to range from ca. 23 to 29% (Table S1).

With respect to the USAXS and SAXS features, it is important to note that the same scattering features are also observed in the DCA and 4CP solvent-swollen wet gels, prior to solvent extraction (see Figure S2 in the Supporting Information). This observation indicates that the general scattering features of the aerogels are characteristic of the inherent wet gel morphology and are not significantly perturbed by the solvent extraction methods.

SAXS profiles of aerogels are typically fit using models originally derived by Beaucage,[58] with careful Porod analysis in order to extract information about the surface characteristics.[57] To extract quantitative dimensions associated with the two scattering features of the aerogels, the USAXS/SAXS data were analyzed using the Unified Fit model,[58] as described in the Supporting Information, with fit parameters listed in Tables 1 and 2. For the aerogels prepared from the DCA and 4CP solutions, the radius of gyration, $R_{g,1}$, for the SAXS scattering feature around q = 0.035 $Å^{-1}$ was found to be in the range of 5−7 nm. Aerogels prepared from SC-dried DCA gels generally

Table 1. Guinier Radius (R_g) and Porod Exponent (P) Values Obtained from Application of the Unified Fit Model to PEEK/DCA Aerogel Scattering Profiles

specimen	$R_{g,2}$ (nm)	P_2	$R_{g,1}$ (nm)	P_1
8% DCA SC	156	3.0	6.3	4.0
10% DCA SC	178	3.5	7.3	4.0
15% DCA SC	138	3.2	7.2	4.0
20% DCA SC	131	2.9	6.6	4.0
8% DCA FD	91	2.6	4.8	4.0
10% DCA FD	87	2.6	4.9	4.0
15% DCA FD	81	2.3	5.4	4.0
20% DCA FD	125	2.6	5.1	4.0

DOI: 10.1021/acsami.9b09699
ACS Appl. Mater. Interfaces 2019, 11, 31508−31519

Table 2. Guinier Radius (R_g) and Porod Exponent (P) Values Obtained from Application of the Unified Fit Model to PEEK/4CP Aerogel Scattering Profiles

specimen	$R_{g,2}$ (nm)	P_2	$R_{g,1}$ (nm)	P_1
8% 4CP SC	262	2.9	5.4	4.0
10% 4CP SC	387	3.4	5.4	4.0
15% 4CP SC	120	3.1	5.3	4.0
20% 4CP SC	194	3.1	5.1	4.0
8% 4CP FD	371	3.2	5.2	4.0
10% 4CP FD	319	3.1	5.1	4.0
15% 4CP FD	233	2.7	4.9	4.0
20% 4CP FD	204	3.1	5.2	4.0

showed an increase in $R_{g,1}$ with increasing gel concentration, while the $R_{g,1}$ values for the freeze-dried DCA gels were relatively constant at ca. 5 nm. For the aerogels prepared from 4CP, the $R_{g,1}$ values were all in the vicinity of 5.2 nm, regardless of the solvent extraction method. For all of the aerogels, the Porod exponents associated with the $R_{g,1}$ feature were found to be constant at P_1 = 4.0, characteristic of scattering features with smooth interfaces.

The radius of gyration, $R_{g,2}$, for the USAXS scattering feature near q = 0.001 Å^{-1} was found to vary in the range of 80−380 nm for all aerogels in this study (Tables 1 and 2). Because the void spaces between the lamellar agglomerates seen in Figures 2 and 3 are generally larger than 1 μm, this scattering feature near q = 0.001 Å^{-1} is tentatively attributed to the lamellar agglomerates. In agreement with the FE-SEM results above, the aerogels prepared from 4CP yielded larger $R_{g,2}$ values relative to the aerogels prepared from DCA. For the DCA aerogels, the $R_{g,2}$ values were significantly larger for the SC-dried samples than that of the freeze-dried samples, consistent with compaction of the agglomerates during the freeze-drying process. However, in contrast to the FE-SEM results, this trend was not observed for the 4CP aerogels, where both sets yielded similar $R_{g,2}$ values. Given the very different forms of the freeze-dried 4CP agglomerates (compacted platelets, Figure 2c) as compared to the SC-dried agglomerates (globular stacks of lamella, Figure 3c), it is likely that a unique structural packing factor consideration is needed to refine the $R_{g,2}$ estimates for the freeze-dried 4CP data sets. This consideration, however, requires a complex customization of the Unified Fit model and is beyond the scope of this general comparison.

The Porod exponents, P_2, associated with the $R_{g,2}$ scattering feature range between 2.3 and 3.5 (Tables 1 and 2). According to fractal geometry, surface fractals are known to exhibit Porod exponents of noninteger values between 3 and 4, whereas noninteger values between 1 and 3 are expected for mass fractals.[56,58,59] Thus, as is generally common for aerogels, the interfacial characteristics of these nanostructured PEEK aerogels are best described as surface fractals with a strong tendency to form mass fractal morphologies. As will be shown below, the fractally rough surfaces of these aerogels will have a profound effect on the surface area and interfacial properties.

Although the tentative assignment of the USAXS scattering feature to the lamellar agglomerates agrees well with the real space FE-SEM data, the precise assignment of the SAXS scattering feature near q = 0.035 Å^{-1} is more ambiguous. For example, the $R_{g,1}$ values listed in Tables 1 and 2 are consistent with the lamellar dimensions commonly observed with PEEK. However, the loss of phase information with X-ray scattering precludes the elimination of an alternative assignment to that of small voids within the agglomerates (i.e., void space around and between the stacked lamella). In attempt to distinguish between these two possible origins of the SAXS feature near q = 0.035 Å^{-1}, we have employed the contrast-matching method available with SANS.

Neutron scattering contrast-matching techniques are often employed to elucidate the morphological origins of scattering features.[60,61] Conveniently, hydrogen (H) and deuterium (D) have very different neutron scattering length densities (SLD), such that the exact ratio of H/D in the solvent imbibed in a porous structure can be tailored to match the SLD of a feature of interest.[61] Scattering intensity is directly proportional to contrast, $(\Delta\rho)^2$, so that the magnitude of scattering features is diminished to extinction when the SLD of the scattering object is matched with the solvent surrounding around it.

SANS experiments were performed on PEEK gels in which the chlorinated gelation solvent was exchanged with either pure H_2O, pure D_2O, or a precise mixture of H_2O and D_2O that was chosen to match the SLD of crystalline PEEK (SLD = 2.71 × 10^{10} cm^{-2}). In this analysis, a mixture of H_2O/D_2O in the ratio 51.4:48.6 (v/v) was used to effectively mask the scattering contributions from crystalline PEEK (see the Supporting Information). The SANS profiles displayed in Figure 6 show the scattering from three different PEEK

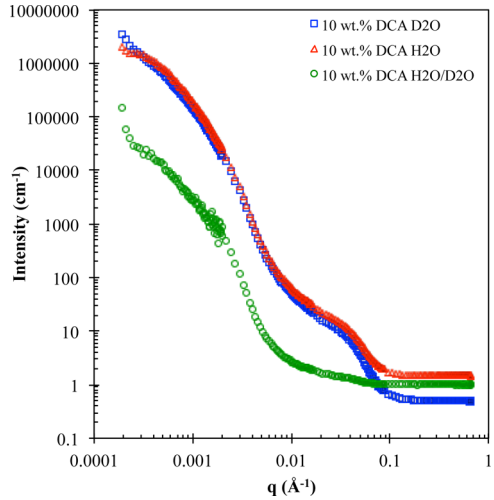

Figure 6. SANS profiles of PEEK gel networks imbibed with either pure D_2O (blue squares), pure H_2O (red triangles), or 51.4:48.6 (v/v) H_2O/D_2O mixture (green circles). All gels were prepared via solvent-exchanging 10 wt % PEEK gels prepared in DCA.

hydrogels formed from a 10 wt % DCA gel that was solvent-exchanged with pure H_2O, pure D_2O, and the precise H_2O/D_2O mixture. For the H_2O and D_2O hydrogel samples, the SANS profiles are essentially identical to that of the corresponding aerogel SAXS profile in Figure 4a. In comparison, however, the SANS profile for the hydrogel containing the 51.4:48.6 (v/v) mixture of H_2O and D_2O shows a near complete elimination of the scattering feature near q = 0.035 Å^{-1}. Similar behavior is observed for other hydrogel compositions, as shown in Figures S5 and S6. Thus, this convenient SANS method of contrast matching confirms an SLD match between the liquid matrix and the crystalline PEEK lamella and provides conclusive evidence that the scattering maximum near q = 0.035 Å^{-1} is attributed to the lamellar morphology of the gels.

DOI: 10.1021/acsami.9b09699
ACS Appl. Mater. Interfaces 2019, 11, 31508−31519

With the SANS confirmation that the SAXS feature near q = 0.035 Å^{-1} originates from the lamellar morphology of PEEK within the gel network, it is now no surprise that the Porod exponent associated with this scattering feature (P_1) is equal to 4.0 (Tables 1 and 2). Scattering intensity proportional to q^{-4} is characteristic of smooth surfaces as expected for the sharp difference in electron density at the crystalline−amorphous interface of the lamellar surfaces. Thus, with respect to the overall hierarchical morphology of these aerogels, this detailed scattering analysis indicates that these materials are ordered over length scales spanning Angstroms (WAXD, Bragg dimensions of crystalline order) to nanometers (SAXS, lamellar features and interlamellar pores) to sub-micrometer (USAXS, multilamellar aggregates with mass fractal interfacial features).

Porosity and Surface Area of PEEK Aerogels. Nitrogen adsorption using the Brunauer−Emmett−Teller (BET) method probes surface area, pore structure, and pore size distribution, as a method to compliment the microstructural understanding gained from SEM and SAXS. The BET method directly measures surface area, which is dependent on accessibility of the surfaces to the nitrogen molecules. PEEK aerogel surface area measurements obtained using the BET method[62] are plotted in Figure 7 as a function of aerogel

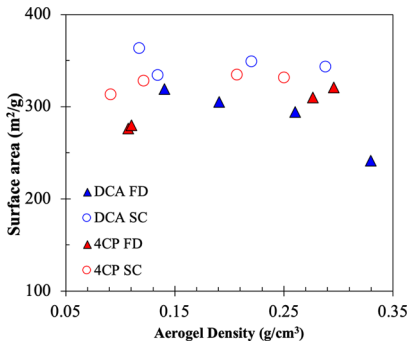

Figure 7. Relationship between BET surface area (m^2/g) and aerogel density (g/cm^3) with respect to the gelling solvent and solvent extraction method.

density (Table S2). All aerogels exhibited high surface areas, up to 365 m^2/g. For both solvents, it is clear that the SC-dried aerogel surface areas are significantly higher than that of their freeze-dried analogues. The freeze-drying process is difficult to control, leading to pore collapse and subsequent densification of the material, which prevents access by the adsorption molecules and consequently lower surface area measurements by BET. Thus, nitrogen adsorption measures the useful, or accessible, material surface area, and supercritical fluid extraction yields a more open and accessible surface within the aerogel structure. This morphological observation is a critical distinction between solvent removal methods, as it pertains to the practical applications of aerogels. Aerogels as functional materials, such as the catalyst support[36] and filtration processes,[39] require high accessible surface area, whereas bulk density is the predominant morphological concern in thermal insulation applications.[63]

Representative BET isotherms from PEEK aerogels obtained by freeze-drying or supercritical fluid extraction to remove the solvent from 15 wt % PEEK gels in DCA or 4CP are shown in Figure 8. The forms of all the isotherms are identical and consistent with an IUPAC type IV mesoporous structure

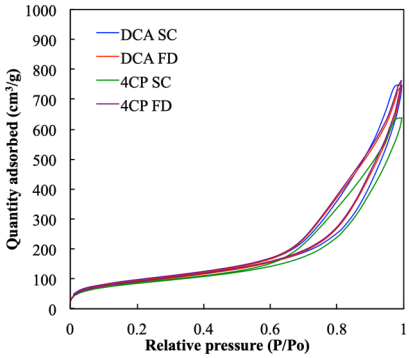

Figure 8. BET adsorption−desorption isotherms of aerogels from freeze-drying or SC-drying PEEK/DCA and PEEK/4CP gels.

consisting of 2−50 nm pores.[64] Futhermore, the hysteresis loop is characteristic of IUPAC H3 hysteresis, which indicates that the mesopores are slit-like and originate from aggregates of plate-like particles.[64] The general size and slit-like shape of the pores suggested by the BET isotherm suggests that nitrogen adsorption is probing the internal porosity of the crystalline agglomerates (Figures 2 and 3) and certainly not the very large pores (of several hundred nm) between the agglomerates. Based on the stacked lamellar morphology observed from the micrographs and SAXS analysis of the SC-dried gels, it is evident that the pores probed by BET are the interlamellar amorphous regions, which are inherently slit-like aggregates of plate-like particles.

The BET method of nitrogen adsorption can also be used to obtain the size distribution of pores. Figure 9 illustrates the

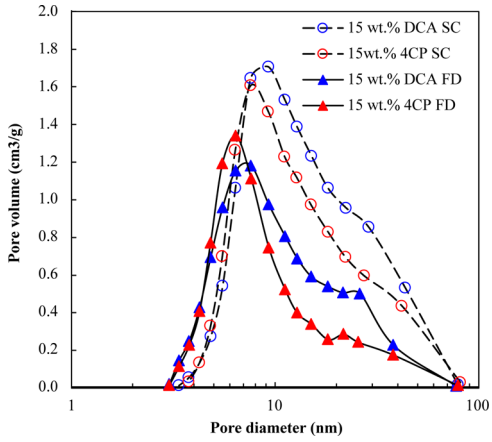

Figure 9. BET pore size distribution of aerogels from freeze-drying or SC-drying PEEK/DCA and PEEK/4CP gels.

pore size distribution of the mesopores in PEEK aerogels prepared by freeze-drying or supercritical fluid extraction to remove solvent from 15 wt % PEEK gels in either DCA or 4CP. In comparing the two gelling solvents, it is evident that the pore size distribution of the PEEK/4CP aerogels is shifted to a lower pore size than the distribution obtained from the PEEK/DCA aerogels. This shift to lower pore sizes for the PEEK/4CP aerogels is the same for both drying techniques. Moreover, the size distribution of pores in both freeze-dried aerogels exhibits a maximum in the pore size distribution of approximately 7 nm, whereas the maximum in the distribution for the SC-dried aerogels is shifted to a larger dimension of around 9 nm. This shift to a larger pore size in supercritically

DOI: 10.1021/acsami.9b09699
ACS Appl. Mater. Interfaces 2019, 11, 31508−31519

dried aerogels is consistent with the more open (less compacted) morphology visible in the SEM micrographs of the SC-dried aerogels (Figure 3).

The BET data in Figure 9 also show that the pore volumes for the freeze-dried aerogels are significantly lower than that of the SC-dried aerogels. The reduced pore volume for the freeze-dried aerogels is further evidence that the freeze-drying method significantly perturbs the gel morphology via densification of mesopores. Local densification in the inter-lamellar amorphous regions also leads to bulk densification of the aerogel specimen. In the aerogel density versus gel concentration plot in Figure 10, both solvents and drying

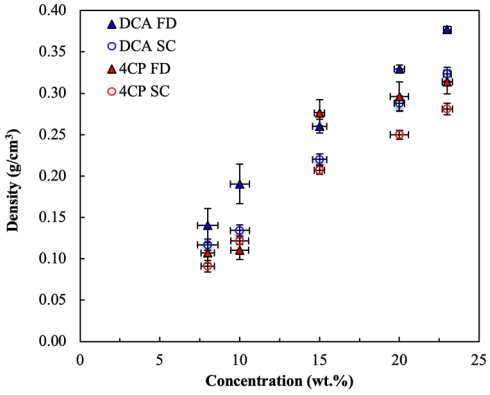

Figure 10. Relationship between PEEK aerogel bulk density (g/cm^3) and PEEK/solvent gel concentration (wt %). No gelation occurs below 4 wt %. Gels prepared in DCA are shown in blue, and gels prepared in 4CP are shown in red. The gel drying technique is denoted as FD (freeze-drying) and SC (supercritical fluid extraction).

methods follow similar linear relationships; however, freeze-dried aerogels from either solvent consistently exhibit higher densities than their supercritically dried analogues.

Another valuable aerogel property directly related to the morphological characteristics of the hierarchical, nanostructured network of agglomerated particles is the overall porosity. PEEK aerogel porosity, Π, was determined using the relationship

$$\Pi = \frac{\frac{1}{\rho_b} - \frac{1}{\rho_s}}{\frac{1}{\rho_b}} \times 100\% \quad (2)$$

where ρ_b is the aerogel bulk density and ρ_s is the skeletal density defined as

$$\rho_s = \frac{X_c\rho_c + (100 - X_c)\rho_a}{100} \quad (3)$$

where ρ_c is the density of crystalline PEEK (1.400 g/cm^3),[65] ρ_a is the density of amorphous PEEK (1.265 g/cm^3),[66] and X_c is the % crystallinity determined by X-ray diffraction (Table S1). As shown in Figure 11, PEEK aerogels are highly porous, up to 93% porosity. As is typical for aerogels,[67] the porosity tracks linearly with aerogel density, which depends primarily on the gel concentration (polymer loading). The porosity is also found to be independent of the solvent type or solvent extraction method. It is interesting to note, however, that although aerogels from PEEK/4CP gels are comprised of a lower volume fraction of crystalline lamella, a lower skeletal density, and slightly lower pore diameters as probed by BET,

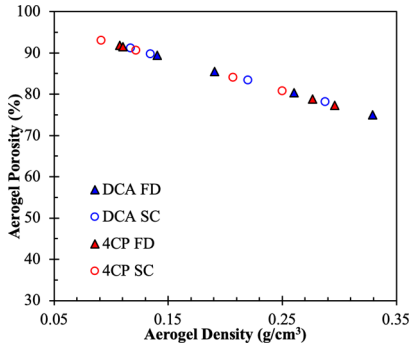

Figure 11. Aerogel porosity vs aerogel bulk density. All aerogels were prepared from PEEK/DCA and PEEK/4CP gels via SC-drying or freeze-drying.

the PEEK/4CP aerogels exhibit porosities identical to that of aerogels prepared from PEEK/DCA solutions. This suggests that the larger macropores between the lamellar agglomerates (Figures 2 and 3) formed during liquid−liquid phase separation in the gelation process are largely responsible for the overall porosity of these PEEK aerogels.

Mechanical and Interfacial Properties of PEEK Aerogels. Morphological differences among PEEK aerogels prepared using different solvent or drying methods do not necessarily extend to differences in mechanical or physical properties. The common power law relationship[68,69] between compressive modulus and aerogel density shown in Figure 12

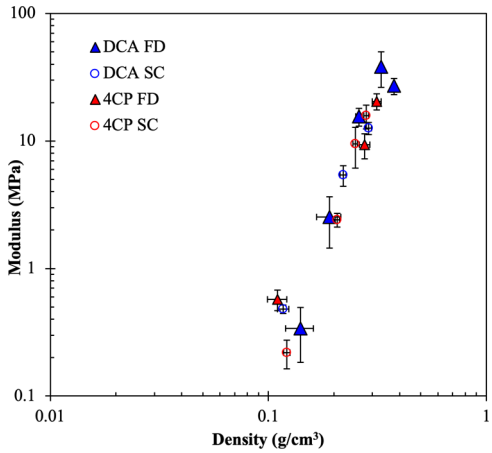

Figure 12. Relationship between compressive modulus and bulk density. Gels prepared in DCA are shown in blue, and gels prepared in 4CP are shown in red. The gel drying technique is denoted as FD (freeze-drying) and SC (supercritical fluid extraction).

is conserved across the solvent type or drying method. The power law relationship demonstrated by the aerogels probed in this study is consistent with the relationship between compressive modulus and aerogel density we reported previously in a study of gelation temperature, annealing, and gel concentration,[5] which further supports the conclusion that aerogel density primarily determines compressive modulus in semicrystalline aerogels of a particular polymer.

In addition to the desirable tunable mechanical properties of PEEK aerogels, the various morphologies available from selection of gel concentration, gelation solvent, and drying method lead to interesting interfacial properties. We have previously shown that the hierarchical morphologies similar to

DOI: 10.1021/acsami.9b09699
ACS Appl. Mater. Interfaces 2019, 11, 31508−31519

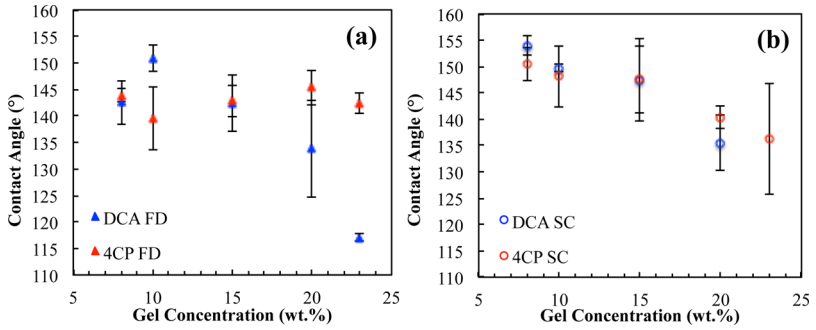

Figure 13. Relationship between aerogel contact angle and gel concentration. Aerogels prepared from PEEK/DCA gels are shown in blue and those prepared from PEEK/4CP gels are shown in red. Data are grouped according to drying technique, either freeze-drying (a) or supercritical CO_2 extraction (b).

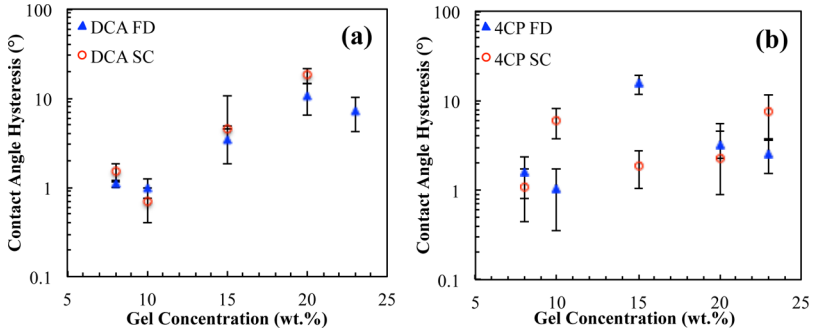

Figure 14. Relationship between aerogel CAH and gel concentration. Aerogels prepared from freeze-drying are shown in blue and aerogels from supercritical fluid extraction are shown in red.

those shown in Figures 2 and 3 from aerogels prepared by freeze-drying PEEK/DCA gels impart bulk hydrophobic and superhydrophobic character on PEEK aerogel monoliths.[5] The inherent water contact angle of semicrystalline PEEK is 63°;[70] however, construction of a hierarchical morphology through physical gelation and subsequent solvent removal imparts sufficient surface roughness to increase the water contact angle up to and beyond 150° on the surface of PEEK aerogels. In addition, the mass fractal morphology observed by SAXS analysis likely contributes to the enhanced water contact angles.

The water contact angles for the aerogels prepared form PEEK/DCA and PEEK/4CP gels are plotted with respect to gel concentration in Figure 13. Superhydrophobic character, as observed by some of the aerogels, can be achieved through the Cassie–Baxter state, in which sufficient surface roughness due to the air-filled micro- and nanoscale hierarchical features reduces the area of the surface–water interface.[71] As expected, aerogels prepared from the lowest concentrations exhibit the highest water contact angles because of their very high porosities and surface areas. Similarly, aerogels prepared by supercritical extraction yield the highest contact angles, consistent with their higher surface areas relative to the freeze-dried aerogels. The systematic relationship between aerogel contact angle and gel concentration for the supercritically dried PEEK aerogels (Figure 13b) indicates that hydrophobicity increases with decreasing concentration, in a relatively tunable fashion. In contrast, the wettability of freeze-dried PEEK aerogels is not tunable (Figure 13a).

The Cassie–Baxter state hydrophobicity and superhydrophobicity are manifested by high water contact angles (superhydrophobic >150°) and low contact angle hysteresis (CAH), generally below 10°.[72] The relationship between aerogel CAH and gel concentration is shown in Figure 14. While the CAH values are observed to increase with gel concentration, it is important to note that the aerogels prepared from low gel concentrations (below 10 wt %) exhibit remarkably low CAH values near or even below 1°. As a comparison to a more widely studied semicrystalline, aromatic polymer aerogel system, sPS aerogels of lower density (0.06 g/mL) yield a CAH value of 10°.[73]

CONCLUSIONS

The full extent of the sol–gel transition of PEEK in 4CP, within the solubility limit, has been demonstrated. The resulting phase diagram shows behavior consistent with a UCST sol–gel transition. This is now the second instance of monolithic thermoreversible gelation of PEEK. Highly porous (up to 93% porosity) PEEK aerogels ranging in density from 0.08 to 0.4 g/cm^3 were prepared from PEEK gels by varying the weight fraction of PEEK dissolved in either 4CP or DCA. Scattering and adsorption data suggest that the hierarchical morphology of these aerogels is composed of a network of solid agglomerates of crystalline lamella with varying degrees of shape and local order that appear to be influenced by the polymer–solvent interaction parameter and drying method. Gelation in DCA produces globular features, whereas gelation in 4CP, a better solvent for PEEK, produces aerogels with platelet-like features comprised of more ordered crystalline lamella.

Freeze-drying appears to densify the morphological features of PEEK aerogels, resulting in overall higher density aerogels than those prepared from SC-drying at comparable wet gel concentration. On a comparable density basis, aerogels prepared from variable solution concentrations, gelation

DOI: 10.1021/acsami.9b09699
ACS Appl. Mater. Interfaces 2019, 11, 31508–31519

solvents, and drying methods showed superimposable compressive modulus versus density trends, leading to the conclusion that density is the governing property with respect to the PEEK aerogel modulus. Additionally, we have shown that PEEK aerogels formed from lower concentration gels in either solvent can exhibit a superhydrophobic character with water contact angles greater than 150° and CAH values near 1°.

■ ASSOCIATED CONTENT

Supporting Information

The Supporting Information is available free of charge on the ACS Publications website at DOI: 10.1021/acsami.9b09699.

X-ray and neutron scattering analysis including data fitting, contrast matching methods, and model details (PDF)

■ AUTHOR INFORMATION

Corresponding Author

*E-mail: rbmoore3@vt.edu. Phone (540) 231-6015. Fax (540) 231-8517.

ORCID

Samantha J. Talley: 0000-0002-9415-1824
Baochau A. Nguyen: 0000-0003-0330-4280
Robert B. Moore: 0000-0001-9057-7695

Present Address

⊥Chemical Diagnostics and Engineering Group, Los Alamos National Laboratory, Los Alamos, New Mexico 87545.

Author Contributions

The manuscript was written through contributions of all authors. All authors have given approval to the final version of the manuscript. R.B.M. developed the intellectual concept and supervised this research. S.L.V., B.A.N., and M.A.B.M. performed supercritical fluid extraction and nitrogen adsorption measurements. A.R. designed and performed all neutron scattering experiments. S.J.T. prepared all materials and performed all other experiments. R.B.M. and S.J.T. designed all other experiments, analyzed all experimental data, and wrote the report.

Notes

The authors declare no competing financial interest.

■ ACKNOWLEDGMENTS

This material is based upon work supported by the National Science Foundation under grant nos. DMR-1507245 and DMR-1809291. This research used resources of the Advanced Photon Source (APS), a U.S. Department of Energy (DOE) Office of Science User Facility operated for the DOE Office of Science by Argonne National Laboratory under General User Proposal number 49574. USAXS/SAXS/WAXD data were collected on the 9-ID-C beamline at the APS, Argonne National Laboratory. This research utilized resources of the Jülich Centre for Neutron Science (JCNS) at Heinz Maier-Leibnitz Zentrum (MLZ) under Proposal number 13716. Neutron scattering data were collected at beamline KWS-2 at the MLZ. Supercritical fluid extraction and BET measurements were conducted at the National Aeronautics and Space Administration (NASA) Glenn Research Center.

■ REFERENCES

(1) Guenet, J.-M. *Thermoreversible Gelation of Polymers and Biopolymers*; Academic Press: London, 1992.
(2) Nijenhuis, K. t. *Thermoreversible Networks*, 1st ed.; Springer: Verlag Berlin Heidelberg, 1997; p 267.
(3) Daniel, C.; Dammer, C.; Guenet, J.-M. On the Definition of Thermoreversible Gels: the Case of Syndiotactic Polystyrene. *Polymer* **1994**, *35*, 4243−4246.
(4) Talley, S. J.; Yuan, X.; Moore, R. B. Thermoreversible Gelation of Poly(ether ether ketone). *ACS Macro Lett.* **2017**, *6*, 262−266.
(5) Talley, S. J.; AndersonSchoepe, C. L.; Berger, C. J.; Leary, K. A.; Snyder, S. A.; Moore, R. B. Mechanically robust and superhydrophobic aerogels of poly(ether ether ketone). *Polymer* **2017**, *126*, 437−445.
(6) Mutin, P. H.; Guenet, J. M. Physical Gels from PVC: Aging and Solvent Effects on Thermal Behavior, Swelling, and Compression Modulus. *Macromolecules* **1989**, *22*, 843−848.
(7) Berghams, H.; Donkers, A.; Frenay, L.; Stoks, W.; De Schryver, F. E.; Moldenaers, P.; Mewis, J. Thermoreversible Gelation of Syndiotactic Poly(methyl methacrylate). *Polymer* **1987**, *28*, 97−102.
(8) Buyse, K.; Berghmans, H.; Bosco, M.; Paoletti, S. Mechanistic Aspects of the Thermoreversible Gelation of Syndiotactic Poly(methyl methacrylate) in Toluene. *Macromolecules* **1998**, *31*, 9224−9230.
(9) Saiani, A.; Spěváček, J.; Guenet, J.-M. Phase Behavior and Polymer/Solvent Interactions in Thermoreversible Gels of Syndiotactic Poly(methyl methacrylate)†. *Macromolecules* **1998**, *31*, 703−710.
(10) Bush, P. J.; Pradhan, D.; Ehrlich, P. Lamellar Structure and Organization in Polyethylene Gels Crystallized From Supercritical Solution in Propane. *Macromolecules* **1991**, *24*, 1439−1440.
(11) Daniel, C.; Longo, S.; Guerra, G. High Porosity Polyethylene Aerogels. *Polyolefins J.* **2015**, *2*, 49−55.
(12) Matsuda, H.; Inoue, T.; Okabe, M.; Ukaji, T. Study of Polyolefin Gel in Organic Solvents I. Structure of Isotactic Polypropylene Gel in Organic Solvents. *Polym. J.* **1987**, *19*, 323.
(13) Guenet, J.-M.; Parmentier, J.; Daniel, C. Porous Materials from Polyvinylidene Fluoride/Solvent Molecular Compounds. *Soft Mater.* **2011**, *9*, 280−294.
(14) Dikshit, A. K.; Nandi, A. K. Thermoreversible Gelation of Poly(vinylidene flouride) in Diethyl Adipate: A Concerted Mechanism. *Macromolecules* **1998**, *31*, 8886−8892.
(15) Aharoni, S. M.; Charlet, G.; Delmas, G. Investigation of solutions and gels of poly(4-methyl-1-pentene) in cyclohexane and decalin by viscosimetry, calorimetry, and x-ray diffraction. A new crystalline form of poly(4-methyl-1-pentane) from gels. *Macromolecules* **1981**, *14*, 1390−1394.
(16) Charlet, G.; Delmas, G. "Modification V" of Poly 4-Methylpentene-1 From Cyclopentane Solutions and Gels. *Polym. Bull.* **1982**, *6*, 367−373.
(17) Charlet, G.; Hong Phuong Nguyen, H. P.; Delmas, G. Thermoreversible gelation of poly(4-methyl-1-pentene) in cyclopentane and cyclohexane. *Macromolecules* **1984**, *17*, 1200−1208.
(18) Daniel, C.; Vitillo, J. G.; Fasano, G.; Guerra, G. Aerogels and Polymorphism of Isotactic Poly(4-methyl-pentene-1). *ACS Appl. Mater. Interfaces* **2011**, *3*, 969−977.
(19) Aubert, J. H. Isotactic Polystyrene Phase Diagrams and Physical Gelation. *Macromolecules* **1988**, *21*, 3468−3473.
(20) Daniel, C.; Menelle, A.; Brulet, A.; Guenet, J.-M. Thermoreversible Gelation of Syndiotactic Polystyrene in Toluene and Chloroform. *Polymer* **1997**, *38*, 4193−4199.
(21) Daniel, C.; Avallone, A.; Guerra, G. Syndiotactic Polystyrene Physical Gels: Guest Influence on Structural Order in Molecular Complex Domains and Gel Transparency. *Macromolecules* **2006**, *39*, 7578−7582.
(22) Roels, T.; Deberdt, F.; Berghmans, H. In *Thermoreversible Gelation in Syndiotactic Polystyrene/Solvent Systems*; Steinkopff: Darmstadt, 1996; pp 82−85.

DOI: 10.1021/acsami.9b09699
ACS Appl. Mater. Interfaces 2019, 11, 31508−31519

(23) Daniel, C.; Deluca, M. D.; Guenet, J.-M.; Brûlet, A.; Menelle, A. Thermoreversible Gelation of Syndiotactic Polystyrene in Benzene. *Polymer* **1996**, *37*, 1273−1280.
(24) De Rudder, J.; Berghmans, H.; De Schryver, F. C.; Bosco, M.; Paoletti, S. Gelation Mechanism of Syndiotactic Polystyrene in Bromoform. *Macromolecules* **2002**, *35*, 9529−9535.
(25) Li, Y.; Xue, G. Molecular Conformation of Syndiotactic Polystyrene Gel from Octadecyl Benzoate Solution. *Macromol. Rapid Commun.* **1998**, *19*, 549−552.
(26) Daniel, C.; Alfano, D.; Guerra, G.; Musto, P. Physical Gelation of Syndiotactic Polystyrene in the Presence of Large Molar Volume Solvents Induced by Volatile Guests of Clathrate Phases. *Macromolecules* **2003**, *36*, 1713−1716.
(27) Orler, E. B.; Yontz, D. J.; Moore, R. B. Sulfonation of Syndiotactic Polystyrene for Model Semicrystalline Ionomer Investigations. *Macromolecules* **1993**, *26*, 5157−5160.
(28) Prasad, A.; Marand, H.; Mandelkern, L. Supermolecular Morphology of Thermoreversible Gels Formed From Homogeneous and Heterogeneous Solutions. *J. Polym. Sci., Part B: Polym. Phys.* **1993**, *31*, 1819−1835.
(29) Mochizuki, J.; Sano, T.; Tokami, T.; Itagaki, H. Decisive Properties of Solvent Able to Form Gels with Syndiotactic Polystyrene. *Polymer* **2015**, *67*, 118−127.
(30) Pierre, A. C.; Pajonk, G. M. Chemistry of Aerogels and Their Applications. *Chem. Rev.* **2002**, *102*, 4243−4266.
(31) Fricke, J.; Tillotson, T. Aerogels: Production, Characterization, and Applications. *Thin Solid Films* **1997**, *297*, 212−223.
(32) Hrubesh, L. W. Aerogel Applications. *J. Non-Cryst. Solids* **1998**, *225*, 335−342.
(33) Yu, Z.-L.; Yang, N.; Apostolopoulou-Kalkavoura, V.; Qin, B.; Ma, Z.-Y.; Xing, W.-Y.; Qiao, C.; Bergström, L.; Antonietti, M.; Yu, S.-H. Fire-Retardant and Thermally Insulating Phenolic-Silica Aerogels. *Angew. Chem., Int. Ed.* **2018**, *57*, 4538−4542.
(34) Owens, B. B.; Passerini, S.; Smyrl, W. H. Lithium Ion Insertion in Porous Metal Oxides. *Electrochim. Acta* **1999**, *45*, 215−224.
(35) Gao, H.; Zhou, T.; Zheng, Y.; Liu, Y.; Chen, J.; Liu, H.; Guo, Z. Integrated Carbon/Red Phosphorus/Graphene Aerogel 3D Architecture via Advanced Vapor-Redistribution for High-Energy Sodium-Ion Batteries. *Adv. Energy Mater.* **2016**, *6*, 1601037.
(36) Pajonk, G. M. Aerogel Catalysts. *Appl. Catal.* **1991**, *72*, 217−266.
(37) Fu, G.; Yan, X.; Chen, Y.; Xu, L.; Sun, D.; Lee, J.-M.; Tang, Y. Boosting Bifunctional Oxygen Electrocatalysis with 3D Graphene Aerogel-Supported Ni/MnO Particles. *Adv. Mater.* **2018**, *30*, 1704609.
(38) Chaudhary, J. P.; Vadodariya, N.; Nataraj, S. K.; Meena, R. Chitosan-based Aerogel Membrane for Robust Oil-In-Water Emulsion Separation. *ACS Appl. Mater. Interfaces* **2015**, *7*, 24957−24962.
(39) Zhai, C.; Jana, S. C. Tuning Porous Networks in Polyimide Aerogels for Airborne Nanoparticle Filtration. *ACS Appl. Mater. Interfaces* **2017**, *9*, 30074−30082.
(40) Tamon, H.; Ishizaka, H.; Yamamoto, T.; Suzuki, T. Influence of Freeze-Drying Conditions on the Mesoporosity of Organic Gels as Carbon Precursors. *Carbon* **2000**, *38*, 1099−1105.
(41) Ren, L.; Cui, S.; Cao, F.; Guo, Q. An Easy Way To Prepare Monolithic Inorganic Oxide Aerogels. *Angew. Chem., Int. Ed.* **2014**, *53*, 10147−10149.
(42) Ilavsky, J.; Jemian, P. R.; Allen, A. J.; Zhang, F.; Levine, L. E.; Long, G. G. Ultra-small-angle X-ray scattering at the Advanced Photon Source. *J. Appl. Crystallogr.* **2009**, *42*, 469−479.
(43) Ilavsky, J.; Zhang, F.; Allen, A. J.; Levine, L. E.; Jemian, P. R.; Long, G. G. Ultra-Small-Angle X-ray Scattering Instrument at the Advanced Photon Source: History, Recent Development, and Current Status. *Metall. Mater. Trans. A* **2013**, *44*, 68−76.
(44) Ilavsky, J. Nika: Software for Two-Dimensional Data Reduction. *J. Appl. Crystallogr.* **2012**, *45*, 324−328.
(45) Ilavsky, J.; Jemian, P. R. Irena: Tool Suite for Modeling and Analysis of Small-angle Scattering. *J. Appl. Crystallogr.* **2009**, *42*, 347−353.
(46) Zhang, F.; Ilavsky, J.; Long, G. G.; Quintana, J. P. G.; Allen, A. J.; Jemian, P. R. Glassy Carbon as an Absolute Intensity Calibration Standard for Small-angle Scattering. *Metall. Mater. Trans. A* **2010**, *41*, 1151−1158.
(47) Radulescu, A.; Szekely, N. K.; Appavou, M.-S. KWS-2: Small Angle Scattering Diffractometer. *J. Large Scale Res. Facil.* **2015**, *1*, 29.
(48) Radulescu, A.; Szekely, N. K.; Appavou, M.-S.; Pipich, V.; Kohnke, T.; Ossovyi, V.; Staringer, S.; Schneider, G. J.; Amann, M.; Zhang-Haagen, B.; Brandl, G.; Drochner, M.; Engels, R.; Hanslik, R.; Kemmerling, G. Studying Soft-matter and Biological Systems over a Wide Length-scale from Nanometer and Micrometer Sizes at the Small-angle Neutron Diffractometer KWS-2. *J. Visualized Exp.* **2016**, *118*, 54639.
(49) Coniglio, A.; Stanley, H. E.; Klein, W. Site-Bond Correlated-Percolation Problem: A Statistical Mechanical Model of Polymer Gelation. *Phys. Rev. Lett.* **1979**, *42*, 518−522.
(50) Okabe, M.; Wada, R.; Tazaki, M.; Homma, T. The Flory-Huggins Interaction Parameter and Thermoreversible Gelation of Poly(vinylidene fluoride) in Organic Solvents. *Polym. J.* **2003**, *35*, 798−803.
(51) Miller-Chou, B. A.; Koenig, J. L. A review of polymer dissolution. *Prog. Polym. Sci.* **2003**, *28*, 1223−1270.
(52) Barton, A. F. M. *CRC Handbook of Solubility Parameters and Other Cohesion Parameters*, 2nd ed.; CRC Press: New York, 1991.
(53) Pietrzynska, M.; Adamska, K.; Szubert, M.; Voelkel, A. Solubility parameter used to predict the effectiveness of monolithic in-needle extraction (MINE) device for the direct analysis of liquid samples. *Anal. Chim. Acta* **2013**, *805*, 54−59.
(54) van Krevelen, D. W. *Properties of Polymers*, 3rd ed.; Elsevier: New York, 1990.
(55) Lakes, R. Materials with structural hierarchy. *Nature* **1993**, *361*, 511−515.
(56) Schaefer, D. W.; Keefer, K. D. Structure of Random Porous Materials: Silica Aerogel. *Phys. Rev. Lett.* **1986**, *56*, 2199−2202.
(57) Pekala, R. W.; Schaefer, D. W. Structure of Organic Aerogels. 1. Morphology and Scaling. *Macromolecules* **1993**, *26*, 5487−5493.
(58) Beaucage, G.; Schaefer, D. W. Structural Studies of Complex Systems Using Small-Angle Scattering: a Unified Guinier/Power-Law Approach. *J. Non-Cryst. Solids* **1994**, *172−174*, 797−805.
(59) Beaucage, G. Small-Angle Scattering from Polymeric Mass Fractals of Arbitrary Mass-Fractal Dimension. *J. Appl. Crystallogr.* **1996**, *29*, 134−146.
(60) Clarkson, C. R.; Solano, N.; Bustin, R. M.; Bustin, A. M. M.; Chalmers, G. R. L.; He, L.; Melnichenko, Y. B.; Radliński, A. P.; Blach, T. P. Pore Structure Characterization of North American Shale Gas Reservoirs Using USANS/SANS, Gas Adsorption, and Mercury Intrusion. *Fuel* **2013**, *103*, 606−616.
(61) Hedden, R. C.; Lee, H.-J.; Bauer, B. J. Characterization of Nanoporous Low-kThin Films by Small-Angle Neutron Scattering Contrast Variation. *Langmuir* **2004**, *20*, 416−422.
(62) Brunauer, S.; Emmett, P. H.; Teller, E. Adsorption of Gases in Multimolecular Layers. *J. Am. Chem. Soc.* **1938**, *60*, 309−319.
(63) Koebel, M.; Rigacci, A.; Achard, P. Aerogel-based Thermal Superinsulation: An Overview. *J. Sol-Gel Sci. Technol.* **2012**, *63*, 315−339.
(64) Alothman, Z. A Review: Fundamental Aspects of Silicate Mesoporous Materials. *Materials* **2012**, *5*, 2874−2902.
(65) Lee, Y.; Porter, R. S. Crystallization of poly(ether ether ketone) oriented by solid-state extrusion. *Macromolecules* **1991**, *24*, 3537−3542.
(66) Blundell, D. J.; Osborn, B. N. The Morphology of Poly(aryl-ether-ether-ketone). *Polymer* **1983**, *24*, 953−958.
(67) Du, M.; Mao, N.; Russell, S. Control of porous structure in flexible silicone aerogels produced from methyltrimethoxysilane (MTMS): the effect of precursor concentration in sol-gel solutions. *J. Mater. Sci.* **2016**, *51*, 719−731.

DOI: 10.1021/acsami.9b09699
ACS Appl. Mater. Interfaces 2019, 11, 31508−31519

(68) Fricke, J. Aerogels - highly tenuous solids with fascinating properties. *J. Non-Cryst. Solids* **1988**, *100*, 169−173.
(69) Nguyen, B. N.; Meador, M. A. B.; Medoro, A.; Arendt, V.; Randall, J.; McCorkle, L.; Shonkwiler, B. Elastic Behavior of Methyltrimethoxysilane Based Aerogels Reinforced with Tri-Isocyanate. *ACS Appl. Mater. Interfaces* **2010**, *2*, 1430−1443.
(70) Ha, S.-W.; Hauert, R.; Ernst, K.-H.; Wintermantel, E. Surface Analysis of Chemically-Etched and Plasma-Treated Polyetheretherketone (PEEK) for Biomedical Applications. *Surf. Coat. Technol.* **1997**, *96*, 293−299.
(71) Quéré, D. Non-Sticking Drops. *Rep. Prog. Phys.* **2005**, *68*, 2495.
(72) Xiu, Y.; Zhu, L.; Hess, D. W.; Wong, C. P. Hierarchical Silicon Etched Structures for Controlled Hydrophobicity/Superhydrophobicity. *Nano Lett.* **2007**, *7*, 3388−3393.
(73) Wang, X.; Jana, S. C. Tailoring of Morphology and Surface Properties of Syndiotactic Polystyrene Aerogels. *Langmuir* **2013**, *29*, 5589−5598.

DOI: 10.1021/acsami.9b09699
ACS Appl. Mater. Interfaces 2019, 11, 31508−31519